Dalton Transactions

ROYAL SOCIETY OF CHEMISTRY

PAPER

View Article Online
View Journal | View Issue

Cite this: *Dalton Trans.*, 2026, **55**, 2855

Isomers of 2,2′:6′,2″-terpyridine and 2,6-dipyrazin-2-ylpyridine with aliphatic substituents: synthesis, coordination chemistry, and catalytic and anticancer activities

Guoqi Zhang, *[a] Haiyu Mei,[a] Amy Kanina,[a] Marilyn Chocho,[a] Paulina Hiyaev,[a] Shu-Yuan Cheng*[a] and Michelle C. Neary [b]

While the synthesis of 4′-aryl substituted 2,2′:6′,2″-terpyridine and its common isomer 4,2′:6′,4″-terpyridine is trivial using the one-pot Krönke condensation procedure, their 4′-alkyl substituted ligands have been sparsely approached. 2,2′:4′,2″-Terpyridine and 4,2′:4′,4″-terpyridine as their rare isomers have only been reported in a few examples as unexpected byproducts during the synthesis of their 4′-aryl derivatives. Likewise, a closely related ligand of 2,2′:6′,2″-terpyridine, 2,6-dipyrazin-2-ylpyridine containing an aliphatic substituent, is unknown to us, and its isomer 4,6-dipyrazin-2-ylpyridine is yet to be discovered. In this work, we employed simple one-pot reactions between an aliphatic aldehyde and 4-acetylpyridine or 2-acetylpyrazine and reported for the first time the synthesis and structural characterization of several aliphatically substituted 4,2′:4′,4″-terpyridine and 2,6-dipyrazin-2-ylpyridine isomers as major products (**3–5**). Two possible intermediates featuring dearomatized structures (**6** and **7**) from similar reactions at lower temperatures were uncovered based on X-ray structural analysis. We assumed that the reaction temperature was critical in determining the major products in each of the reactions. We further investigated their coordination chemistry with various zinc and cobalt salts by isolating crystals of three complexes (**8–10**) of these new ligands and clarifying their solid-state structures by X-ray crystallography. Both a one-dimensional (1-D) polymeric chain of Zn^{II} (**8**) and a 2-D network of Co^{II} (**9**) with the divergent ligand, 4′-^{t}Bu-4,2′:4′,4″-terpyridine (**3**), were characterized, along with a mononuclear Co^{II} complex (**10**) of 4-^{t}Bu-2,6-dipyrazin-2-ylpyridine (**4**). The new metal complexes were examined for preliminary catalytic performance in the hydroboration and hydrosilylation reactions of styrene, highlighting the potential of complex **10** as an active catalyst for both reactions, even though the regioselectivity remains to be improved through further ligand modification and/or condition optimization. Finally, the biopharmaceutical application of these new compounds as potent anticancer agents has been explored, and the *in vitro* toxicity studies suggest that among all new compounds tested, metal complexes (**8** and **9**) based on isomer **3** are promising drug candidates against breast cancer cells MCF-7 and MDA-MB-468, while they showed lower toxicity levels towards the non-tumorigenic epithelial cell, MCF-10, compared to cisplatin.

Received 25th November 2025,
Accepted 9th January 2026

DOI: 10.1039/d5dt02824h

rsc.li/dalton

1. Introduction

Terpyridines are a class of important organic compounds consisting of three pyridine rings linked *via* single bonds.[1,2] Among the 48 possible isomeric structures of terpyridines, 2,2′:6′,2″-terpyridine (2,2′:6′,2″-tpy) is the one that has been most extensively studied, owing to its strong metal binding ability that allows for the formation of stable metal coordination complexes with most metal ions across the periodic table.[3–5] As a versatile building block, it has also shown great potential for applications in supramolecular and materials chemistry.[6–10] As documented in a recent report by Constable and Housecroft,[11] the synthetic ease of 2,2′:6′,2″-tpy derivatives (and their divergent analogues such as substituted 3,2′:6′,4″-terpyridines and 4,2′:6′,4″-terpyridines)[12] is likely the main reason for them to be so popularly observed in the literature. Their synthesis is usually trivial and it employs the well-known Krönke reaction for the preparation of the aromatically substituted 4′-position of 2,2′:6′,2″-tpy.[13] However, unexpected products were often observed from either the process of the

[a]*Department of Sciences, John Jay College and Ph.D. Program in Chemistry, The Graduate Center of the City University of New York, New York, 10019 NY, USA. E-mail: guzhang@jjay.cuny.edu, shcheng@jjay.cuny.edu*
[b]*Department of Chemistry, Hunter College, the City University of New York, New York, 10065 NY, USA*

Claisen–Schmidt condensation of 2-acetylpyridine with an aromatic aldehyde or the facile one-pot approach by the direct reaction between two equivalents of 2-acetylpyridine and the aromatic aldehyde in the presence of a source of ammonia (**a**, Scheme 1).[11] Typically, undesired products including various diketones, triketones and even cyclohexane derivatives have been reported.[11] Notably, a closely related isomer of 2,2′:6′,2″-tpy, 2,2′:4′,2″-terpyridine (2,2′:4′,2″-tpy) could also be the product from the one-pot procedure, revealed in sporadic reports when the aldehyde was *p*-tolualdehyde or benzaldehyde.[14–18] This is presumably attributed to the 1,2-addition of the enol or enolate of 2-acetylpyridine with the carbonyl group of the enone intermediate formed by the initial reaction between an aldehyde and 2-acetylpyridine (**b**, Scheme 1). In addition, a singular example of a related isomer of a divergent analog, 4′-phenyl-4,2′:4′,4″-tpy, was also observed during the preparation of 4′-phenyl-4,2′:6′,4″-tpy from benzaldehyde and 4-acetylpyridine.[19]

Besides, the facile one-pot Kröhnke condensation has been extended to the synthesis of other terpyridine derivatives such as 2,6-bis(pyrazin-2-yl)pyridines by replacing 2-acetylpyridine with 2-acetylpyrazine containing additional N-donating sites.[20–22] Because this one-pot procedure usually requires the use of aromatic aldehydes, the resulting products are limited to 4′-aryl derivatives and hence 2,2′:6′,2″-tpys or 2,6-dipyrazin-2-ylpyridines with aliphatic substituents are extremely rare.[23–26] To our knowledge, only two examples, namely 4′-*tert*-butyl-2,2′:6′,2″-tpy (**1**, Scheme 2) and 4′-*tert*-butyl-4,2′:6′,4″-tpy (**2**, Scheme 2), have been thus far reported using Kröhnke condensation.[27,28] Aliphatically substituted 2,2′:4′,2″-tpy, 4,2′:4′,4″-tpy, 2,6-dipyrazin-2-ylpyridines or 4,6-dipyrazin-2-ylpyridines are unknown.

We have long been interested in the synthesis, structures, reactivity and metal coordination chemistry of 2,2′:6′,2″-tpy and 4,2′:6′,4″-tpy derivatives, with a particular focus on the observation of novel metal catalysts and active anticancer and antifungal drugs.[29–36] In this contribution, we wish to report on our recent success in the one-pot synthesis of the rare isomer of 2,2′:6′,2″-tpy, 4,2′:4′,4″-tpy as well as 2,6-dipyrazin-2-ylpyridines (or 4,6-dipyrazin-2-ylpyridines) with an aliphatic substituent on the central pyridine ring (compounds **3–5**, Scheme 2), along with the serendipitous observation of two possible intermediates (**6** and **7**) during the unusual cyclization process towards the formation of compounds **3** and **5**. Furthermore, their metal coordination chemistry with Zn^{II} and Co^{II} is explored for the first time and their preliminary catalytic properties and anticancer activities against two kinds of breast cancer cell lines are studied as well.

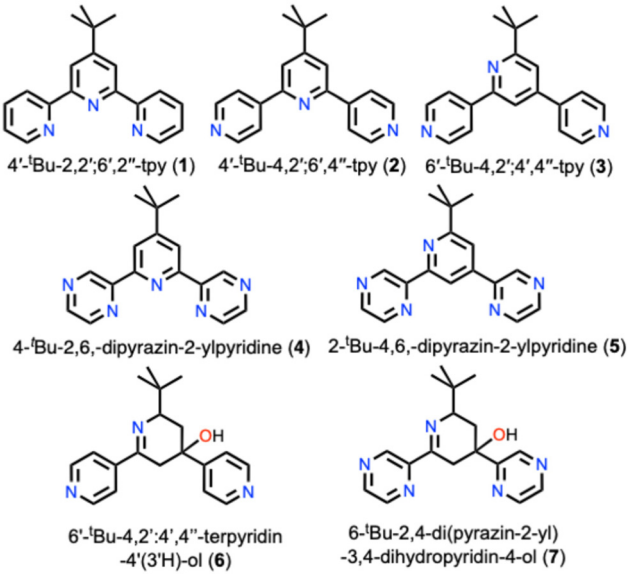

Scheme 2 The structures of known compounds **1** and **2** and new compounds **3–7** studied in this work.

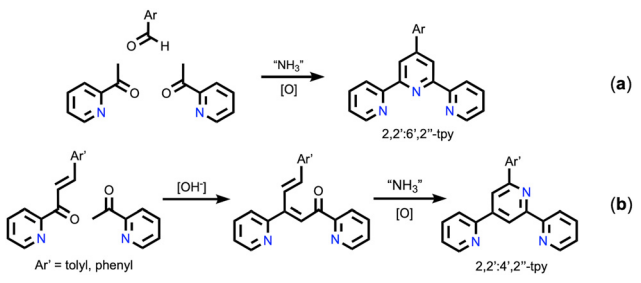

Scheme 1 One-pot synthetic routes to 2,2′:6′,2″-tpy and 2,2′:4′,2″-tpy.

2. Results and discussion

2.1 Synthesis of 6′-*tert*-butyl-2,2′:4′,2″-tpy (3) and 6′-*tert*-butyl-5′,6′-dihydro-[4,2′:4′,4″-terpyridin]-4′(3′*H*)-ol (6)

Previously, both 4′-*tert*-butyl-2,2′:6′,2″-tpy (**1**) and 4′-*tert*-butyl-4,2′:6′,4″-tpy (**2**) have been synthesized from a one-pot reaction between pivaldehyde and two equivalents of 2-acetylpyrazine in an aqueous ethanol solution in the presence of an excess amount of aqueous ammonia under refluxing conditions.[27,28] We were curious whether high temperature was necessary to accomplish the reactions, as it was known that aromatically 4′-substituted 2,2′:6′,2″-tpy or 4,2′:6′,4″-tpy compounds have been usually synthesized at room temperature. Therefore, we initiated our goal for novel ligand synthesis in this work by implementing the same method reported, yet at lower temperatures, to hopefully uncover the effect of temperature on the product formation. Thus, the reaction of two equiv. of 4-acetylpyridine and pivalaldehyde was first carried out in EtOH by adding 1.2 equiv. of solid KOH and then an excess amount of aqueous ammonia and the reaction mixture was allowed to react at 65 °C for three days (Fig. 1 and see the Experimental section for details). To this end, pale yellow microcrystals of **3** were harvested directly from the reaction mixture as a suspension in an appreciable yield (~48%), significantly higher than that for **1** and **2**. Previously, the highest yield of 15% was obtained for the synthesis of similarly isomeric 6′-tolyl-

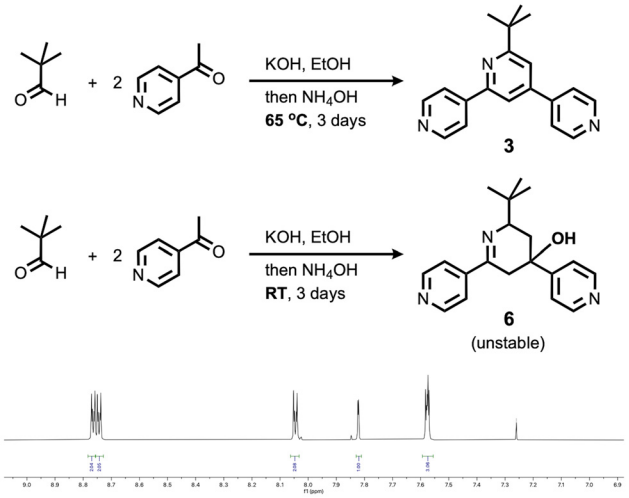

Fig. 1 The partial ^{1}H NMR spectrum of **3** shown for protons in the aromatic region in $CDCl_3$.

2,2′:4′,2″-tpy at much higher temperatures (120–160 °C).[37] The product as collected was found to have good purity in solution and its ^{1}H NMR spectrum in $CDCl_3$ clearly reveals an unsymmetrical terpyridine backbone consistent with the molecular structure of **3** shown in Scheme 2 (Fig. 1), unlike that observed for the closely related compound **2** with symmetrical aromatic H signals.[27] The ^{13}C NMR spectrum with 11 distinct carbon signals in the aromatic region further supports its unsymmetrical structure. The UV-Vis spectrum of **3** in CH_2Cl_2 solution shows an absorption peak at 244 nm with a broad shoulder centered at 298 nm, owing to a ligand-centered n → π* transition from the tpy domain (Fig. S1, SI).

Crystals of **3** suitable for X-ray diffraction analysis were grown from a CH_2Cl_2/MeOH solution by slow evaporation and its single-crystal structure has been determined as shown in Fig. 2. While the structural refinement was not of high quality, due probably to the fact that the achiral yet unsymmetrical molecules were packed with some intermolecular polarity and so the crystal grew as an inversion twin, the atomic location and connectivity were clearly revealed, which is consistent with the structure determined above by NMR spectroscopy in solution.

Next, we attempted to conduct the same reaction as that for **3** at room temperature to see whether the same product could be approached (Fig. 1). From this reaction, we were also able to collect the white solid product that precipitated out from the reaction solution in an appreciable amount. However, its solution NMR spectra (in $CDCl_3$) showed a complicated mixture, which could not be purified by column chromatography. Attempts to crystallize the product in MeOH/H_2O solution occasionally (two out of five trials) led to the observation of a small amount of colorless plate-like crystals that are suitable for X-ray diffraction analysis. Thus, this crystal structure has been unambiguously determined to be the novel compound (**6**) shown in Scheme 2, and its molecular structure is displayed in Fig. 2. Compound **6** crystallizes in the triclinic space group $P\bar{1}$ and key bond parameters are presented in the caption of Fig. 2. While two stereogenic centers (C23 and C25) exist in the structure, the centrosymmetric space group reveals a racemic mixture of two enantiomers in the crystal chosen for analysis. The presence of a hydroxyl group on the central non-aromatic imine ring was unprecedented, and it reveals a completely new structure from one-pot Kröhnke condensation that has never been reported so far. Each ligand molecule co-crystallizes with one water molecule to form a one-dimensional double-chained hydrogen-bonded framework. Specifically, three distinct hydrogen bonds were formed between the hydroxyl group, the water molecule and two pyridyl-N atoms of the ligand (see Fig. S16, SI). Unfortunately, we were unable to obtain a pure enough sample for solution NMR measurements by using column chromatography. We collected the ^{1}H NMR spectrum in $CDCl_3$ with a small amount of single crystals of **6**, but it suggested the presence of a mixture of at least four different compounds, possibly indicating the poor stability of **6** in solution or the concurrent crystallization of similar compounds such as regioisomers.

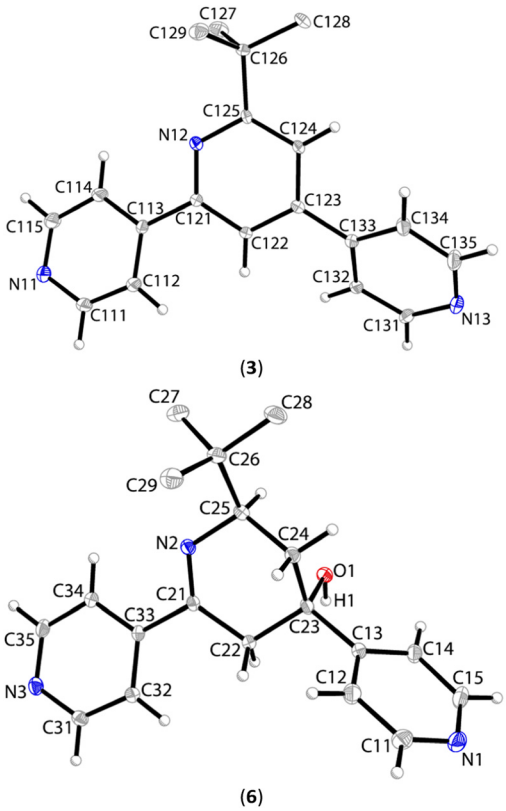

Fig. 2 The crystal structures of compounds **3** and **6** with atomic displacement parameters drawn at the 30% probability level. H atoms on the ^{t}Bu group are omitted for clarity. Selected bond parameters of **6**: C21–N2 = 1.274(2), C25–N2 = 1.474(2), C21–C22 = 1.505(2), C22–C23 = 1.529(2), C23–C24 = 1.532(2), C24–C25 = 1.527(2), C25–C26 = 1.552(2), C23–O1 = 1.4259(19), O1–H1 = 0.91(2), C21–C33 = 1.496(2), C23–C13 = 1.528(2), C11–N1 = C15–N1 = 1.331(2), C31–N3 = 1.336(2), and C35–N3 = 1.339(2) Å.

2.2 Synthesis of 4-*tert*-butyl-2,6-dipyrazin-2-ylpyridine (4)

Similarly, we further explored the synthesis of aliphatically substituted 2,6-dipyrazin-2-ylpyridines by introducing a *tert*-butyl group on the central pyridine ring, which has not been reported yet. First, we realized the synthesis of 4-*tert*-butyl-2,6-dipyrazin-2-ylpyridine (**4**) as a regular product from Kröhnke condensation by following a similar procedure for the preparation of **1** and **2**.[27,28] Specifically, it was carried out using a one-pot reaction between pivaldehyde and two equivalents of 2-acetylpyrazine in an aqueous ethanol solution at room temperature for 16 h and then an excess amount of aqueous ammonia was added (Scheme 3). The reaction was conducted then under reflux for an additional 16 h. A pale yellow crude solid was isolated by filtration and purified by recrystallization from a dichloromethane/hexane solution through evaporation. Colorless X-ray quality single crystals of **4** were obtained by slowly evaporating a solution of CH_2Cl_2/hexane. Compound **4** is well soluble in polar organic solvents and was fully characterized by UV-Vis, IR and NMR spectroscopy and high-resolution mass spectrometry (HR-MS). The UV-Vis absorption spectrum in CH_2Cl_2 shows a single broad absorption with a maximum at 290 nm, attributed to the ligand-centered n → π* transition from the 2,6-dipyrazin-2-ylpyridine domain, which is in sharp contrast to the absorptions of **3** with a tpy domain. The IR spectrum reveals peaks between 2961 and 2866 cm^{-1}, corresponding to the C^{sp^3}–H absorption of a *tert*-butyl group in **3**, in addition to the C^{sp^2}–H bond stretching at 3050 cm^{-1}. The moderate peak at 1601 cm^{-1} corresponds to the imine absorption of pyridine rings. The HR-MS spectrum reveals the base peak at 292.1559, consistent with the $[M + H]^+$ species (calc. 292.1562), and the highest peak at 314.1375 for $[M + Na]^+$ (calc. 314.1382) with low abundance. The ^1H NMR spectrum in $CDCl_3$ verifies the molecular structure of **4** in solution, which is consistent with a C_2-symmetric structure.

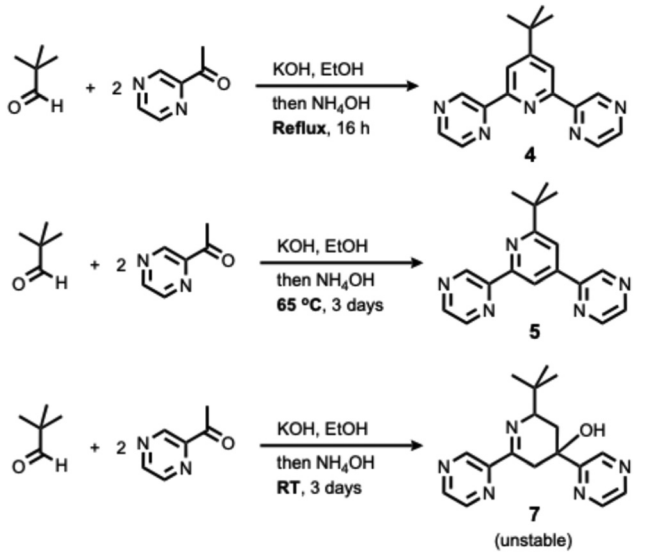

Scheme 3 The comparison of the synthetic procedures of **4**, **5** and **7**.

The solid-state structure of **4**, as shown in Fig. 3, was determined by X-ray crystallographic analysis and its relevant bond parameters are listed in the caption of Fig. 3. Compound **4** crystallizes in the monoclinic space group $P2_1/c$ and in the asymmetric unit there contains one independent molecule. The two side pyrazinyl rings are oriented in a *trans*,*trans*-configuration towards the central pyridine ring with regard to N2 and N4 atoms, which does not offer a convergent N_3 cavity as drawn in Fig. 3, similar to the configuration found in the crystal structure of **1**.[27] All bond distances and angles are unexceptional compared to those found in the molecules of **1** and **2**.[27,28] The planes of three N-heterocycles deviate slightly from coplanarity with distortion angles between the least-squares planes of rings containing N2/N3 and N3/N4 being 9.1(2) and 7.0(2)°, in contrast to the larger distortion angles between the planes of relevant pyridine rings observed in **1** and **2**. The better coplanarity in the molecule of **4** could be attributed to the formation of a one-dimensional hydrogen-bonded network through multiple intermolecular hydrogen bonds, thanks to the existence of an additional N-acceptor on the side pyrazine arms of **4** compared to **1**. Specifically, the hydrogen-bonded network is dominated by a number of non-classical C–H···N hydrogen bonds between the side arms of pyrazine rings as presented in Fig. 4. Three of the total five N atoms participate in the hydrogen bonding interactions, two from one pyrazine arm and one from the other arm. The distances of N···H contacts involved in the H-bonded network are in the range of 2.567–2.741 Å. The central pyridine ring does not participate in the formation of hydrogen bonds.

2.3 Synthesis of 2-*tert*-butyl-4,6-dipyrazin-2-ylpyridine (5) and 2-*tert*-butyl-4,6-di(pyrazin-2-yl)-2,3,4,5-tetrahydropyridin-4-ol (7)

The successful synthesis of unexpected product **3** by increasing the reaction temperature prompts us to further investigate the effect of temperature on the formation of **4**, and thus we performed two more reactions by using the same procedure, yet at

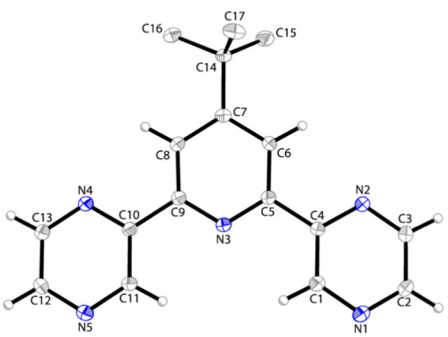

Fig. 3 The crystal structure of **4** with atomic displacement parameters at the 30% probability level. Selected bond lengths: N1–C2 = 1.330(2), N1–C1 = 1.331(2), N2–C4 = 1.335(2), N2–C3 = 1.336(2), N3–C9 = 1.3402 (19), N3–C5 = 1.3454(19), N4–C13 = 1.331(2), N4–C10 = 1.3376(19), N5–C12 = 1.333(2), N5–C11 = 1.334(2), C1–C4 = 1.389(2), C4–C5 = 1.482(2), C9–C10 = 1.486(2), and C7–C14 = 1.531(2) Å.

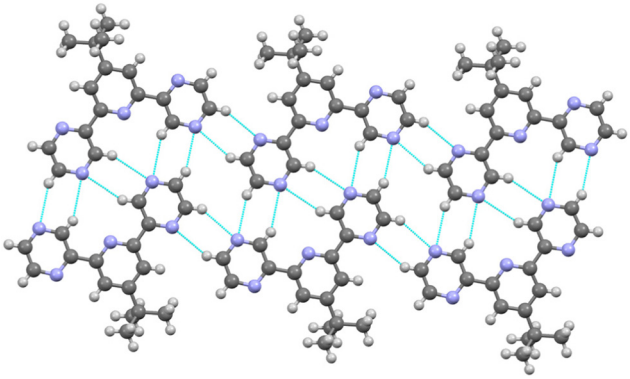

Fig. 4 The ball–stick representation of the one-dimensional hydrogen-bonded polymer found in the packing mode of **4**.

lower temperatures. Again, we conducted two parallel reactions, at 65 °C or room temperature, respectively, over a period of three days (Scheme 3, see details in the Experimental section). First, when the reaction was carried out at 65 °C, like compound **3**, a new product, 2-*tert*-butyl-4,6-dipyrazin-2-ylpyridine (**5**), was isolated in 45.4% yield. Compound **5** displays good solubility in polar organic solvents and was fully characterized by UV-Vis, IR, and NMR spectroscopy and elemental analysis. The UV-Vis spectrum of **5** shows a major absorption band centred at 290 nm with an intensity very close to that found for **4**, indicating that the ligand isomerization at the central pyridine ring has little effect on the electronic configuration (Fig. 1S, SI). The IR spectrum reveals similar absorption to that of **4** with only minor shifts. The solution ^{1}H NMR spectrum of **5** reveals proton signals in the aromatic region consistent with an unsymmetrical structure, in contrast to the fewer peaks found for the symmetrical compound **4** as displayed in Fig. 5.

X-ray quality crystals of **5** were obtained by slowly evaporating a CH_2Cl_2/MeOH solution and its crystal structure was confirmed by X-ray crystallography. Unlike **4**, compound **5** crystallizes in the orthorhombic space group *Pnma* and there are four independent molecules present in the asymmetric unit. Its molecular structure is displayed in Fig. 6 and relevant bond parameters shown in the caption reveal good similarity to those of compound **4** except for the central N atom being placed at a different position. The aromatic rings adopt almost

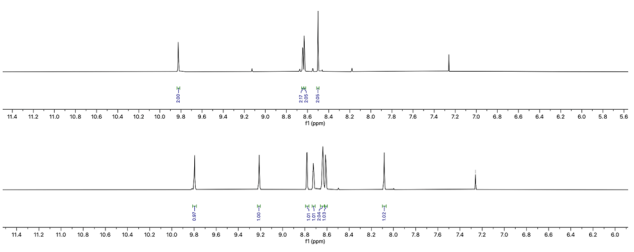

Fig. 5 Comparison of the partial ^{1}H NMR spectrum of compounds **4** (top) and **5** (bottom) for protons in the aromatic region in $CDCl_3$.

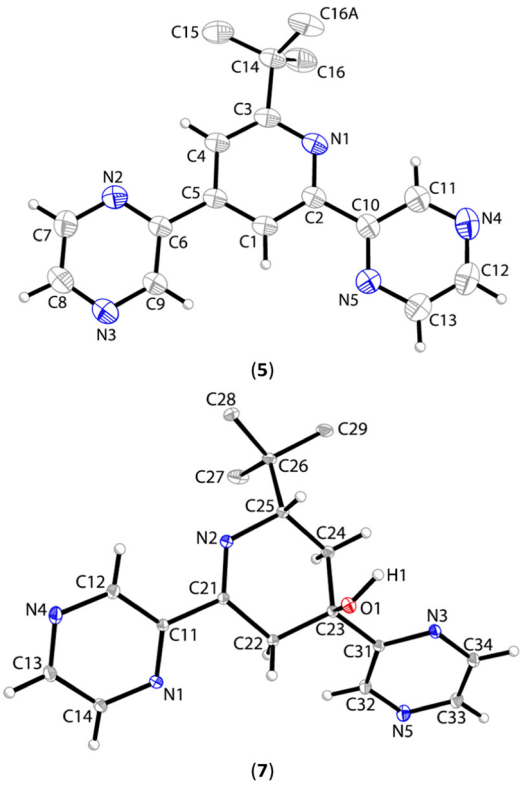

Fig. 6 The crystal structures of **5** and **7** with atomic displacement parameters drawn at the 30% probability level. H atoms on the ^{t}Bu group are omitted for clarity. Selected bond parameters for **5**: N1–C2 = 1.340(4), N1–C3 = 1.341(4), C3–C14 = 1.539(4), C1–C2 = 1.383(4), C1–C5 = 1.382 (4), C3–C4 = 1.384(4), C4–C5 = 1.394(4), N2–C6 = 1.323(4), N2–C7 = 1.327(4), N3–C8 = 1.308(5), N3–C9 = 1.328(4), N4–C11 = 1.332(4), N4–C12 = 1.332(5), N5–C10 = 1.324(4), and N5–C13 = 1.323(4) Å; for **7**: N2–C21 = 1.2773(11), N2–C25 = 1.4661(11), C21–C22 = 1.5082(12), C22–C23 = 1.5146(11), C23–C24 = 1.5378(12), C24–C25 = 1.5286(12), C25–C26 = 1.5539(12), C23–O1 = 1.4306(10), O1–H1 = 0.911(16), C11–C21 = 1.4899 (11), and C23–C31 = 1.5298(12) Å.

perfect coplanarity without measurable distortion angles between the least-squares planes of the rings. Unlike the hydrogen bonding interaction found in the packing mode of **4**, in the crystal of **5** no significant hydrogen bonds were found. Molecules of **5** adopt a columnar packing mode along the crystallographic *b* axis (see Fig. S15, SI). However, no significant π-stacking interactions between the adjacent molecules could be found.

As it was found that reaction temperature has played a critical role in driving the diverse formation between products **2**, **3** and **6** previously, and now between **4** and **5**, we continued to further investigate the reaction between pivaldehyde and 2-acetylpyrazine at room temperature. Thus, when the same reaction leading to **4** was conducted at room temperature, we noticed that a good amount of solid product could be also isolated from the reaction mixture after cooling the solution to 0 °C for one week (see the Experimental section). As observed for compound **6**, the solution NMR spectrum of this crude product revealed a complicated mixture that could not be puri-

fied by column chromatography. Again, we were able to crystallize the crude product from a MeOH/H_2O solution and isolate a small amount of colorless block-like crystals. The structure was well solved by X-ray diffraction analysis and matched that of compound **7** (Scheme 3). Compound **7** crystallizes in the monoclinic space group $P2_1/c$ and relevant bond lengths are shown in the caption of Fig. 6. The bond parameters for the central N-heterocycle are all close to those found in **6**. The asymmetric unit (Fig. 6) contains *R*- and *S*-stereocentres, and the unit cell in the centrosymmetric space group contains both *R*,*S*- and *S*,*R*-enantiomers. Intermolecular O–H···N hydrogen bonds between the hydroxyl group and one of the pyrazinyl-N atoms (N5) dominate the packing mode and are responsible for the formation of one-dimensional hydrogen-bonded chains (see Fig. S17, SI), which is different from that found in the packing mode of **6** (which was instead involved in hydrogen bonding with co-crystallized water). Again, the solution ^{1}H NMR spectrum from the crystalline sample of **7** reveals a complicated mixture of several compounds that could not be identified, indicating its poor stability in solution or a mixture of crystalline products.

2.4 Synthesis of the coordination polymer $[Zn(3)I_2]_n$ (8)

With the new aliphatically substituted ligands (**3–5**) in hand, we were interested to explore their coordination chemistry with transition metals such as zinc and cobalt, and here we report on our preliminary results on the synthesis and crystal structures of three coordination complexes/polymers with ligands **3** and **4**. Previously, the divergent ligand **2** was used to construct diverse coordination polymers with ZnI_2 and $Co(NCS)_2$ salts.[28] To compare with those results, we used the layering method for *in situ* crystallization of products during reactions of ligand **3** and the ZnI_2 salt using a mixture of CH_2Cl_2/MeOH as the solvent in a test tube. After one week at room temperature, colorless block-like crystals were harvested. As the product is insoluble in common organic solvents, solution NMR spectra could not be obtained. The elemental analysis of the crystalline sample suggests a 1 : 1 metal/ligand ratio, referring to an empirical formula of $Zn(3)I_2$. X-ray crystallography was carried out to confirm its solid-state structure as a coordination polymer $[Zn(3)I_2]_n$ (**8**). Polymer **8** crystallizes in the orthorhombic space group *Pbcn*. There exist eight $\{ZnI_2(3)\}$ motifs in the unit cell. Two such motifs are plotted in Fig. 7, showing key metal coordination centers. Each ZnI_2 links with two ligands (one is generated by a symmetry operation) to form an infinite polymeric chain. The Zn ion adopts a tetrahedral geometry and the bond parameters (in the caption of Fig. 7) are unexceptional. The structure of **8** is similar to that of $\{Zn(2)I_2{\cdot}1,2\text{-}Cl_2C_6H_4\}_n$, resulting from the same reaction by using ligand **2** previously,[28] though the latter contains a co-crystallized solvent, 1,2-dichlorobenzene, which participates in the π-stacking interactions with the aromatic rings of ligand **2**. As in $\{Zn(2)I_2{\cdot}1,2\text{-}Cl_2C_6H_4\}_n$, each Zn center in **8** coordinates to two N atoms from the sidearm 4-pyridyl groups, and thus the ligand adopts a divergent two-coordinate mode with the central pyridyl-N atom remaining non-coordinated. The

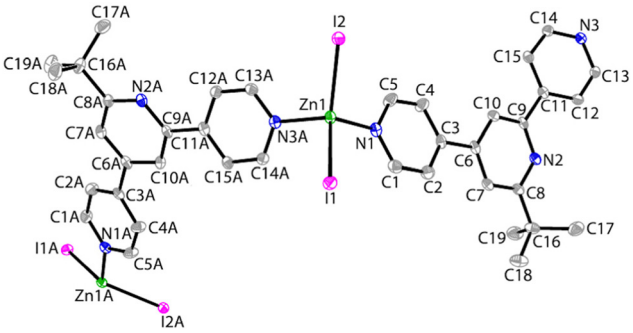

Fig. 7 The crystal structure of two repeating structural units in **8** with atomic displacement parameters drawn at the 30% probability level. H atoms are omitted for clarity. Symmetry code: A = $x + \frac{1}{2}$, $-y + \frac{1}{2}$, $1 - z$. Selected bond parameters about the metal center: Zn1–N1 = 2.072(4), Zn1–N3^i = 2.076(4), Zn1–I1 = 2.5723(6), and Zn1–I2 = 2.5517(6) Å; N1–Zn1–N3^i = 105.67(15), N1–Zn1–I1 = 106.04(11), N1–Zn1–I2 = 107.04 (11), I1–Zn1–N3^i = 105.07(11), I2–Zn1–N3^i = 106.98(11), and I1–Zn1–I2 = 124.68(2)°. Symmetry code: i = $x + \frac{1}{2}$, $-y + \frac{1}{2}$, $1 - z$.

2,2′:4′,2″-tpy domain of ligand **3** deviates slightly from coplanarity and the angles between the least-squares planes of the pyridine rings containing N1/N2 and N2/N3 are 15.0(7) and 16.7(6)°, respectively.

The helical polymeric chain of **8** extends along the crystallographic *a* axis of the unit cell *via* a screw axis, as shown in Fig. 8; this arrangement is similar to other known ZnX_2 assemblies of 4,2′:6′,4″-tpy ligands.[12] The alternate Zn···Zn separation that determines the pitch of the helix is 21.622(2) Å. The helical chains further pack together through π···π interactions between the 4-pyridyl rings (the closest C···C contact is 3.504 (7) Å). In addition, non-classical C–H···π interactions between ^{t}Bu groups and the aromatic rings are also present in the packing mode.

2.5 Synthesis of the coordination network $\{Co(3)_2(NCS)_2{\cdot}2CH_3OH\}_n$ (9)

Following the synthesis of polymer **8**, we investigated the reaction of ligand **3** with $Co(NCS)_2$, in order to compare with the results previously reported on the reaction of the isomer **2** with $Co(NCS)_2$.[28] Crystals of $\{Co(3)_2(NCS)_2{\cdot}2CH_3OH\}_n$ (**9**) were readily formed from the same layering method as that of **8** in one week, and the elemental analysis data are consistent with

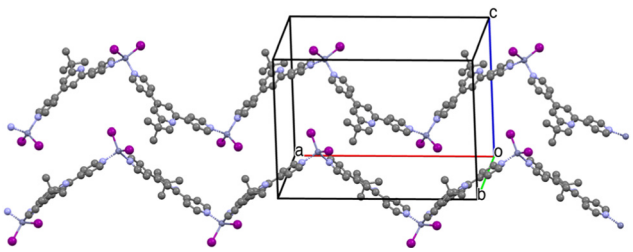

Fig. 8 The partial one-dimensional helical chains found in the packing mode of **8**.

the composition as suggested. The FT-IR spectrum of **9** (recorded as a solid sample) reveals the presence of a thiocyanate ion at 2035 cm^{-1}, along with the absorption of the ligand. The metal–ligand framework was unambiguously determined by X-ray diffraction analysis. However, much of the co-crystallized solvent was disordered and treated as a diffuse contribution to the scattering, so the solvation is not definitive. Complex **9** crystallizes in the monoclinic space group *C*2/*c* and the unit cell contains eight ligand molecules and four $Co(NCS)_2$ centers. Each asymmetric unit contains two independent ligands linked by one $Co(NCS)_2$ unit (Fig. 9), while the two other coordinating ligand molecules are generated over symmetry operations. The reaction of **2** with $Co(NCS)_2$ gave rise to a similar coordination polymer, $[\{\{Co(\mathbf{2})_2(NCS)_2\cdot 1/4CH_3OH\}\cdot H_2O\}_n]$;[28] in which the metal/ligand ratio remains the same (1 : 2) as that found in **9**. In both polymers, the Co^{II} center is octahedrally coordinated to four pyridyl-N atoms of four adjacent ligands and two N atoms from thiocyanate ligands. The bond parameters around the Co atom are unexceptional in both cases. The central pyridyl-N atom of ligand **3** remains uncoordinated as in the other coordination structures discussed here.

Extension of the building block around the hexacoordinate Co^{II} centers and sidearm pyridine rings leads to the formation of a two-dimensional coordination network along the crystallographic *bc* plane (Fig. 10). The network is composed of 4 × 4 grid-like units formed by four ligand molecules and four Co^{II} nodes, which is similar to the structure of $[\{\{4Co(\mathbf{2})_2(NCS)_2\cdot CH_3OH\}\cdot H_2O\}_n]$, indicating the displacement of the central N-atom has little effect on the result of coordination-driven self-assembly. In fact, such a (4, 4) net is an extremely common network for combinations of divergent terpyridines with $Co(NCS)_2$.[38] The diagonal Co···Co distances in the grid units of **9** are 24.007(6) and 11.768(3) Å. The ^{t}Bu groups appear to be above and below the 2D sheet from a side view of the sheet down the crystallographic *a* axis (Fig. 10). These ^{t}Bu groups participate in the formation of non-classical C–H···π hydrogen bonds with ligands from adjacent sheets and dominate the three-dimensional packing pattern in the crystal of **9** (see Fig. S18, SI).

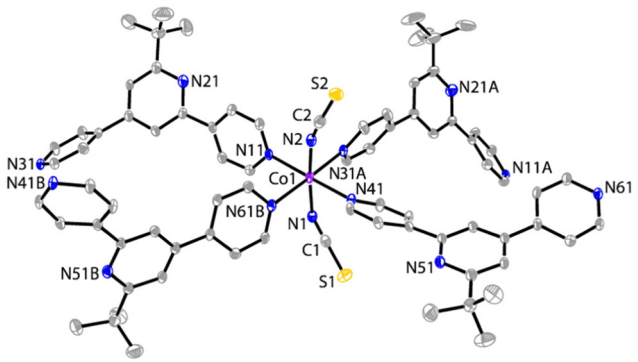

Fig. 9 The crystal structure of the coordination environment for polymer **9** with atomic displacement parameters drawn at the 30% probability level. Solvents and H atoms are omitted for clarity. Symmetry code: A = *x*, −*y* − 2, *z* − ½. Symmetry code: B = *x*, −*y* − 1, *z* + ½. Selected bond parameters: Co1–N11 = 2.182(2), Co1–N41 = 2.165(4), Co1–N1 = 2.095(3), Co1–N2 = 2.069(3), $Co1^i$–N31 = 2.185(2), $Co1^i$–N61 = 2.205(2) Å, N11–Co1–N41 = 177.95(9), N1–Co1–N2 = 173.03(10), and N31–$Co1^i$–N61 = 175.57(9)°. Symmetry code: i = *x*, −*y*, *z* − ½.

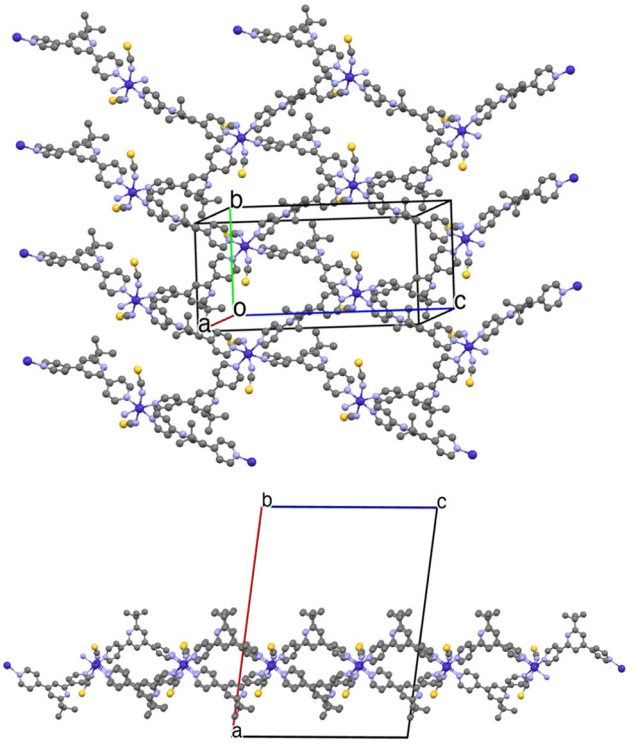

Fig. 10 A 2-D sheet in **9** along the crystallographic *bc* plane (top) and the view through one sheet looking down the *a* axis (bottom).

2.6 Synthesis of the coordination complex $Co(4)Cl_2\cdot C_7H_8$ (10)

The reaction of ligand **4** with $CoCl_2$ at an equimolar ratio of 1 : 2 was carried out using a CH_2Cl_2/MeOH/toluene solvent mixture and green block-like crystals of $Co(\mathbf{4})Cl_2\cdot C_7H_8$ (**10**) were obtained by slow evaporation of the solution over a period of one week. The metal/ligand ratio in **10** was determined to be 1 : 1 by elemental analysis. Complex **10** is partially soluble in CH_2Cl_2 and $CHCl_3$, yet poorly soluble in MeOH, EtOH and toluene. The solution UV-Vis spectrum of **10** shows not only ligand-centered absorption at 236 and 287 nm, but also additional peaks at 331 and 347 nm, attributed to a metal–ligand charge transfer (MLCT) transition state upon metal complexation. The crystal structure of **10** was confirmed by X-ray crystallography as a 1 : 1 mononuclear complex (Fig. 11). Compound **10** crystallizes in a chiral orthorhombic space group $P2_12_12_1$. The unit cell contains four complexes and each cocrystallizes with one molecule of toluene through π···π interactions. Though the molecule itself appears to be achiral, the intermolecular packing, including the positioning of a disordered toluene solvent molecule, broke the symmetry. The ligand serves as a chelating ligand with a Co^{II} center to form a trigonal bipyramidal CoN_3Cl_2 environment, leaving the

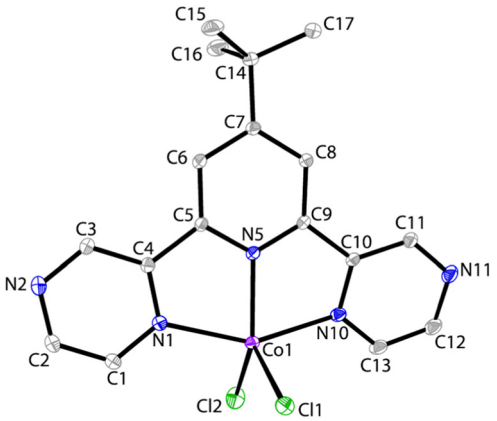

Fig. 11 The molecular structure of **10** with atomic displacement parameters at the 30% probability level. Solvents and H atoms are omitted for clarity. Selected bond parameters for **10**: Co1–N1 = 2.1496(15), Co1–N5 = 2.0450(14), Co1–N10 = 2.1453(15), Co1–Cl1 = 2.2912(6), Co1–Cl2 = 2.2593(6) Å, C1–C5 = 1.382(4), C3–C4 = 1.384(4), C4–C5 = 1.394(4), N2–C6 = 1.323(4), N2–C7 = 1.327(4), N3–C8 = 1.308(5), N3–C9 = 1.328(4), N4–C11 = 1.332(4), N4–C12 = 1.332(5), N5–C10 = 1.324(4), and N5–C13 = 1.323(4) Å; N1–Co1–N5 = 76.15(6), N5–Co1–N10 = 76.06(6), N1–Co1–N10 = 150.84(6), N5–Co1–Cl1 = 112.07(4), N5–Co1–Cl2 = 138.91(4), N1–Co1–Cl1 = 103.46(5), N1–Co1–Cl2 = 96.96(5), N10–Co1–Cl1 = 94.99(4), N10–Co1–Cl2 = 98.15(5), and Cl1–Co1–Cl2 = 108.94(2)°.

outer pyrazinyl-N atoms uncoordinated, which is common in most coordination complexes of 2,6-bis(pyrazin-2-yl)pyridine ligands,[20–22] except in one rare example where a copper atom bridges two mononuclear $CuCl_2$ complexes of 4-phenyl-2,6-bis(pyrazin-2-yl)pyridine to form a dimer by using one of the outer pyrazinyl-N atoms.[20] The bond parameters around the Co atom are unexceptional as depicted in the caption of Fig. 11. Despite the metal complexation, the aromatic region in the ligand still deviates from coplanarity with distortion angles between the least-squares planes of rings containing N1/N5 and N10/N5 being 4.9(3) and 11.0(3)°, comparable to those found above in free ligand **4**. The packing of crystal **10** is dominated by multiple non-classical C–H···Cl hydrogen bonds and no significant π-stacking interaction was observed between molecules of the complex.

2.7 Catalytic properties

Transition metal complexes or coordination networks of tpy ligands have been extensively exploited as catalysts for a variety of organic transformations.[10] In our previous work, both 2,2′:6′,2″-tpy and 4,2′:6′,4″-tpy ligands have been extensively explored for Earth-abundant metal catalysis (such as Co, Mn, Fe, V, *etc.*), with a focus on the hydroboration and hydrosilylation reactions of various unsaturated bonds including alkenes.[29–34] In particular, highly efficient hydroboration of alkenes and ketones has been achieved by using a coordination polymer assembled by $CoCl_2$ and 4′-(4-pyridyl)-2,2′:6′,2″-tpy.[30,31] In order to evaluate whether the new Zn^{II} and Co^{II} complexes **8–10** could be used as catalysts for alkene hydroboration and hydrosilylation, we adopted the optimized reaction conditions previously used for Co-catalysed alkene hydroboration to perform catalytic hydroboration of styrene with pinacolborane (HBpin). The preliminary results of catalytic testing are summarized in Table 1. It was found that when compound **8** (0.5 mol%) and KO^{t}Bu (1 mol%) were combined in THF, the hydroboration of styrene was partially realized at room temperature to give a small amount of alkylboronates including both regioisomers (**11a** and **12a**) with 1 : 9 regioselectivity (entry 1). Under the same conditions, the Co^{II} coordination network **9** was tested as a precatalyst, yet only a trace amount of product was detected (entry 2). This is in sharp contrast with the high catalytic activity displayed by the Co^{II} coordination polymer of 4′-(4-pyridyl)-2,2′:6′,2″-tpy for the same reaction.[30] However, the mononuclear Co^{II} complex **10** showed the highest reactivity and a quantitative yield was obtained in 16 h (entry 3), although the regioselectivity for both regioisomers appeared to be poor (2 : 3). Likewise, the hydrosilylation of styrene with phenylsilane ($PhSiH_3$) was carried out by using complexes **8–10** as precatalysts under the same conditions (entries 4–6). The results revealed that complex **10** was the most effective catalyst affording silylated products (**11b** and **12b**) in a reasonable yield, while the regioselectivity was not ideal (2 : 1). In addition, a control experiment using the $CoCl_2$ salt as a precatalyst was conducted and only negligible conversion was detected (entry 7), indicating the importance of ligands in dominating the catalytic reactivity.

2.8 *In vitro* anticancer activities

Previously, both 2,2′:6′,2″-tpy derivatives and metal complexes have displayed remarkable anticancer activity,[35,36,39,40] and hence we were interested in determining whether the new compounds (ligands **3–5** and complexes **8–10**) are promising drug candidates against selected breast cancer cells in comparison with the clinically approved drug cisplatin. For consist-

Table 1 Catalytic hydroboration or hydrosilylation of styrene using complexes **8–10** as precatalysts[a]

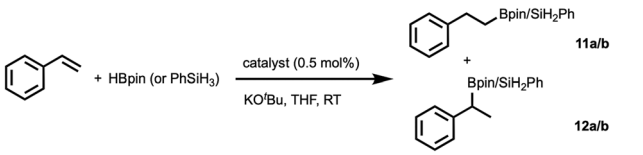

Entry	Catalyst	Hydride	Yield[b]/%	Ratio[b]
1	**8**	HBpin	10	1 : 9 (**11a : 12a**)
2	**9**	HBpin	<5	—
3	**10**	HBpin	>99	2 : 3 (**11a : 12a**)
4	**8**	$PhSiH_3$	Trace	—
5	**9**	$PhSiH_3$	Trace	—
6	**10**	$PhSiH_3$	65	2 : 1 (**11b : 12b**)
7	$CoCl_2$	HBpin	<5	—

[a] Conditions: styrene (1.0 mmol), HBpin or $PhSiH_3$ (1.1 mmol), catalyst (0.5 mol%), additive (1 mol%), THF (0.5 mL), rt, 16 h and under N_2. [b] Determined by GC-MS analysis with hexamethylbenzene as an internal standard, as compared with authentic products.

ency, DMSO was used to dissolve all the compounds (including cisplatin for comparison) and then cell culture media was added to form a homogeneous aqueous solution (see the Experimental section). The *in vitro* cytotoxicity was investigated on human breast cancer cells (MCF-7), triple-negative breast cancer cells (MDA-MB-468) and a non-tumorigenic epithelial cell line from the mammary gland (MCF-10A) using a cell proliferation CCK-8 assay. All the compounds were incubated for 72 h and then the cell viability was evaluated. The results are summarized in Table 2.

Among the ligands tested, compound **3** demonstrated stronger inhibition of cell proliferation compared to **4** and **5**, which did not show notable toxicity across all three tested cell lines. Likewise, complex **10**, which is composed of ligand **4**, also showed very low toxicity against all three cell lines. However, while both complexes **8** and **9** containing ligand **3** and metal ions exhibited much lower toxicity toward the healthy, non-cancerous MDA-10A cells than cisplatin (IC_{50}: 52.93 μM for **8** and 50.75 μM for **9** *vs.* 18.75 μM for cisplatin), both metal assemblies showed remarkable toxicity against both cancer cell lines, which are comparable to cisplatin. Specifically, compound **8** displayed IC_{50} values of 13.30 μM against MCF-7 cells, which is at the same level as cisplatin, although a relatively higher IC_{50} value was detected upon inhibiting MDA-MB-468 cell proliferation in contrast to cisplatin (14.34 *vs.* 5.20 μM). A similar inhibition level was also found for compound **9** towards MDA-MB-468 cells as compared to compound **8**; however, we observed rather strong toxicity while exposing compound **9** to MCF-7 cell lines (IC_{50} = 0.941 μM). Thus, complex **9** was particularly potent in inhibiting MCF-7 cell growth compared to MDA-MB-468 cells. Therefore, the findings here suggest that both complexes **8** and **9** could be promising drug candidates that might outperform cisplatin, as their toxicity against two kinds of breast cancer cells is comparable to that of cisplatin, while remaining less toxic for non-cancerous cells.

2.9 Conclusions

In this work, we present, for the first time, the synthesis and characterization of rare isomers of 2,2′:6′,2″-tpy and 2,6-dipyrazin-2-ylpyridine, namely, 4,2′:4′,4″-tpy and 4,6-dipyrazin-2-ylpyridine with an aliphatic substituent on the central pyridine ring, respectively. The effect of temperature on dominating the formation of different products was explored for the classical one-pot Kröhnke condensation reaction between an aliphatic aldehyde and a ketone. Compared to the regular products, 4′-*tert*-butyl-2,2′:6′,2″-tpy (**1**), 4′-*tert*-butyl-4,2′:6′,4″-tpy (**2**) and 4-*tert*-butyl-2,6-dipyrazin-2-ylpyridine (**4**), obtained under refluxing conditions, their isomers (**3** and **5**) were obtained at a slightly lower reaction temperature (65 °C). On further lowering the temperature (room temperature), we isolated crystals of two possible intermediates with a dearomatized central ring (**6** and **7**), leading to the formation of **3** and **5**, even though their solution structures could not be determined, probably due to their poor stability. The coordination chemistry of these new isomers has been explored and two coordination polymers (1-D Zn^{II} **8** and 2-D Co^{II} **9**) of **3** and one mononuclear Co^{II} complex (**10**) of **4** have been isolated and characterized, while the synthesis of complexes with ligand **5** has been unsuccessful thus far. Preliminary catalytic properties of new metal complexes were investigated in the hydroboration and hydrosilylation reactions of styrene, and the results indicated good catalytic activity of the mononuclear Co^{II} complex (**10**) for both reactions, although the regioselectivity is yet to be improved. The anticancer activity of both ligands **3–5** and complexes **8–10** was studied against two breast cancer cell lines, MCF-7 and MDA-MB-468, as well as a non-cancerous cell line, MCF-10A, and the results were compared with the clinical drug cisplatin. The results reveal that the tpy isomer **3** and its metal assemblies (**8** and **9**) are all toxic against both breast cancer cells, with IC_{50} levels being comparable to that of cisplatin, although **8** and **9** were found to be more friendly towards healthy cells. In contrast, both isomers of 4,6-dipyrazin-2-ylpyridine (**4** and **5**) and the cobalt complex (**10**) based on **4** did not show significant toxicity for all cell lines tested here.

Table 2 Half maximal inhibitory concentration (IC_{50}) values (μM) of compounds **3–5** and **8–10** against the breast cancer cells MCF-7 and MDA-MB-468 and the non-tumorigenic epithelial cell MCF-10A

Compound	MCF-7	MDA-MB-468	MCF-10A
3	3.60 ± 0.53	12.91 ± 0.72	5.49 ± 2.16
4	>100	>100	>100
5	>100	>100	>100
8	13.30 ± 4.46	14.34 ± 1.11	52.93 ± 0.41
9	0.941 ± 0.423	13.22 ± 0.42	50.75 ± 0.47
10	>100	>100	>100
Cisplatin	13.10 ± 2.73	5.20 ± 0.96	18.75 ± 1.42

3. Experimental

3.1 Materials and methods

Unless specified otherwise, the synthesis processes were carried out under ambient conditions in a fumehood. Anhydrous grade solvents and reagents used for catalytic tests were obtained from Aldrich or Fisher Scientific and stored over 4 Å molecular sieves. Other solvents or chemicals of analytical grade, including styrene, are used as received from TCI America or Fisher Scientific without further purification. FT-IR spectra were recorded using a Shimadzu 8400S instrument with solid samples under N_2 using a Golden Gate ATR accessory. Elemental analyses were performed by Midwest Microlab LLC in Indianapolis, USA. ^{1}H NMR and ^{13}C NMR spectra were recorded at room temperature using a Bruker AV 500 or 600 MHz NMR spectrometer, with chemical shifts (δ) referenced to the residual solvent signal. Solution UV-Vis electronic absorption spectroscopy was recorded using a Shimadzu UV-2700 spectrophotometer. HR-MS data were obtained using an Agilent 6550 QToF coupled to an Agilent 1290 Infinity LC system. GC-MS analysis was obtained using a Shimadzu

GCMS-QP2010S gas chromatograph mass spectrometer (column: SHRX1-5MS, thickness: 0.25 m, diameter: 0.25 mm, length: 30.0 m; conditions: 30–200 °C, 10 °C min^{-1}, injection temperature: 100 °C, and solvent cutoff: 3 min).

3.2 Synthetic procedures

3.2.1 Synthesis of 4′-^{t}Bu-2,2′:4′,2″-tpy (3). A solution of 4-acetylpyridine (2.42 g, 20.0 mmol) in EtOH (15 mL) was mixed with pivalaldehyde (0.861 g, 10.0 mmol) in a 250 mL round-bottomed flask equipped with a magnetic stirrer. Solid KOH (0.67 g, 12 mmol) was then added upon rigorous stirring. The mixture turned yellow and then orange within a few minutes. Aqueous ammonia (50 mL, 28%) was then added in one portion. The reaction mixture was heated to 65 °C and allowed to react for 3 days. Pale yellow microcrystals have been collected by filtration upon cooling down the reaction mixture to room temperature. The crystals were washed carefully with an EtOH/H_2O mixture for 3 times and then dried in air. X-ray quality colorless single crystals were obtained by recrystallizing the product from a CH_2Cl_2/MeOH solution by slow evaporation. Yield: 1.38 g (47.7%). M.p.: 177–180 °C. UV/Vis λ_{max}/nm (1.00×10^{-5} mol L^{-1}, CH_2Cl_2) 244 ($\varepsilon/10^3$ dm^3 mol^{-1} cm^{-1} 32.5), 298 (8.0). FT-IR (solid, cm^{-1}): 3033w, 2958m, 1590s, 1537s, 1497w, 1476w, 1400s, 1363m, 1226w, 1169m, 1078m, 993m, 821s, 656m. ^{1}H NMR (500 MHz, $CDCl_3$) δ 8.78–8.76 (m, 2H), 8.76–8.73 (m, 2H), 8.06–8.03 (m, 2H), 7.82 (d, J = 1.4 Hz, 1H), 7.59–7.56 (m, 3H, overlapping), 1.48 (s, 9H) ppm. ^{13}C NMR (126 MHz, $CDCl_3$) δ 171.0, 153.9, 150.8(2C), 150.3(2C), 147.4, 146.8, 121.8(2C), 121.3(2C), 117.4, 115.8, 38.2, 30.3 ppm. Anal. calcd for $C_{19}H_{19}N_3$: C 78.86, H 6.62, N 14.52%. Found C 78.55, H 6.73, N 14.35%.

3.2.2 Synthesis of 4-*tert*-butyl-2,6-di(pyrazin-2-yl)pyridine (4). A solution of 2-acetylpyrazine (2.46 g, 20.0 mmol) in EtOH/H_2O (30 mL, 2 : 1, v/v) was mixed with pivalaldehyde (0.861 g, 10.0 mmol) in a 250 mL round-bottomed flask equipped with a magnetic stirrer. Solid KOH (1.12 g, 20 mmol) was then added upon rigorous stirring. The mixture turned yellow and then red within a few minutes. The mixture was stirred at room temperature for 1 h, after which aqueous ammonia (30 mL, 28%) was added. The reaction mixture was heated to reflux. Yellowish precipitate started to appear after 1 h and the solution was stirred for an additional 16 hours, after which the reaction mixture was allowed to cool to 0 °C and the precipitate was collected by filtration, washed with H_2O and dried *in vacuo*. The pale-yellow solid was recrystallized from a dichloromethane/hexane solution, and colorless crystals were obtained (note: we noticed that there was a minor impurity in product **4** that could not be removed even after recrystallization three times or after purification by column chromatography twice, as detected by NMR spectroscopy). Yield: 0.770 g (26.5%). M.p.: 202–204 °C. UV/Vis λ_{max}/nm (1.00×10^{-5} mol L^{-1}, CH_2Cl_2) 245 ($\varepsilon/10^3$ dm^3 mol^{-1} cm^{-1} 20.0), 290 (24.2). FT-IR (solid, cm^{-1}): 3059w, 2961w, 2866w, 1601m, 1572w, 1544w, 1474s, 1432w, 1379s, 1248s, 1184w, 1121s, 1052m, 1040s, 1017w, 854s, 763m, 689m, 654m. ^{1}H NMR (600 MHz, $CDCl_3$) δ 9.83 (d, J = 1.5 Hz, 2H), 8.65 (dd, J = 2.5, 1.5 Hz, 2H), 8.63 (d, J = 2.5 Hz, 2H), 8.50 (s, 2H), 1.47 (s, 9H) ppm. ^{13}C NMR (126 MHz, $CDCl_3$): δ 162.8, 153.8, 151.2, 144.5, 143.7, 143.5, 119.2, 35.5, 30.7 ppm. HR-MS (ESI positive): 292.1559 ($[M + H]^+$, calcd 292.1562), 314.1375 ($[M + Na]^+$, calcd 314.1382).

3.2.3 Synthesis of 2-*tert*-butyl-4,6-dipyrazin-2-ylpyridine (5). The procedure followed is similar to that for compound **4**, except that the reaction mixture was heated to 65 °C and allowed to react for 3 days. A pale yellow solid was isolated as a precipitate from the resulting solution and washed with an EtOH/H_2O mixture 3 times and then dried in air. X-ray quality colorless single crystals were obtained by recrystallizing the product from a CH_2Cl_2/MeOH solution by slow evaporation. Yield: 1.32 g (45.4%). M.p.: 143–144 °C. UV/Vis λ_{max}/nm (1.00×10^{-5} mol L^{-1}, CH_2Cl_2) 236 ($\varepsilon/10^3$ dm^3 mol^{-1} cm^{-1} 28.8), 290 (25.0). FT-IR (solid, cm^{-1}): 3041w, 2970m, 1604s, 1577w, 1557m, 1523m, 1472s, 1431w, 1371s, 1304w, 1250m, 1140s, 1052m, 1040s, 891m, 843s, 759m, 716w, 677s. ^{1}H NMR (500 MHz, $CDCl_3$) δ 9.80 (d, J = 1.5 Hz, 1H), 9.21 (d, J = 1.6 Hz, 1H), 8.78 (d, J = 1.5 Hz, 1H), 8.72 (dd, J = 2.6, 1.5 Hz, 1H), 8.66–8.62 (m, 2H), 8.61 (d, J = 2.5 Hz, 1H), 8.09 (d, J = 1.5 Hz, 1H), 1.51 (s, 9H). ^{13}C NMR (126 MHz, $CDCl_3$) δ 170.6, 153.9, 151.5, 151.1, 145.2, 144.7, 144.6, 144.5, 143.8, 143.6, 142.8, 117.5, 115.7, 38.2, 30.4. Anal. calcd for $C_{17}H_{17}N_5$: C 70.08, H 5.88, N 24.04%. Found C 70.44, H 5.95, N 23.89%.

3.2.4 Synthesis of 2-*tert*-butyl-4,6-dipyrazin-2-ylpyridine (6). The procedure followed is similar to that of compound **3**, except that the reaction mixture was heated to 65 °C and allowed to react for 3 days. A pale yellow solid was isolated as a precipitate from the resulting solution and washed with an EtOH/H_2O mixture 3 times and then dried in air. A small amount of colourless single crystals was obtained from a MeOH/H_2O solution by slow evaporation. The NMR spectrum of crystalline samples shows the presence of a complicated mixture. Attempts to purify the bulk sample by column chromatography were unsuccessful.

3.2.5 Synthesis of 2-*tert*-butyl-4,6-dipyrazin-2-ylpyridine (7). The procedure followed is that used for compound **4**, except that the reaction mixture was heated to 65 °C and allowed to react for 3 days. A pale yellow solid was isolated as a precipitate from the resulting solution and washed with an EtOH/H_2O mixture 3 times and then dried in air. X-ray quality colourless single crystals were obtained from CH_2Cl_2/hexane solution by slow evaporation. The NMR spectrum of crystalline samples shows the presence of a complicated mixture. Attempts to purify the bulk sample by column chromatography were unsuccessful.

3.2.6 Synthesis of $[Zn(3)I_2]_n$ (8). A solution of **3** (28.9 mg, 0.100 mmol) in MeOH/CH_2Cl_2 (10 mL, 1 : 3, v/v) was placed in a test tube. A blank solution of MeOH/CH_2Cl_2 (4 mL, 1 : 1, v/v) was layered on the top of the ligand solution, followed by a solution of ZnI_2 (31.8 mg, 0.100 mmol) in MeOH (10 mL). The tube was sealed and allowed to stand at room temperature for one week, during which X-ray quality colorless blocks grew at the bottom of the tube. The crystals were collected by decanting the solvent and washed with MeOH and then dried *in vacuo*. Yield: 43.1 mg (71%). FT-IR (solid, cm^{-1}): 2957w, 1615s,

1598s, 1535m, 1502w, 1430w, 1402s, 1362w, 1218s, 1165w, 1063s, 1025s, 826s, 679m, 637s. ^{1}H NMR (400 MHz, DMSO) δ 83.42 (bs), 48.26 (bs), 31.69 (bs), 30.80 (bs), 12.82 (bs), 10.43 (bs), 9.92 (bs) ppm. Anal. calcd for $C_{19}H_{19}I_2N_3Zn$: C 37.50, H 3.15, N 6.90%. Found C 37.76, H 3.24, N 6.74%.

3.2.7 Synthesis of $\{Co(3)_2(NCS)_2{\cdot}2CH_3OH\}_n$ (9). The procedure is similar to that of **8**, except that $Co(NCS)_2$ (17.5 mg, 0.100 mmol) was used. Pink plate-like crystals of **9** were collected in 65% yield (26.5 mg) based on the ligand. FT-IR (solid, cm^{-1}): 3447br, 2963m, 2127s, 2035s, 1615s, 1600s, 1537w, 1401m, 1363w, 1226w, 1018m, 828s, 675m, 634s. Anal. calcd for $C_{40}H_{38}CoN_8S_2{\cdot}CH_3OH$: C 62.66, H 5.39, N 14.26%. Found C 62.45, H 5.52, N 13.96%. Note: the microanalytic data show a small amount of methanol molecules per unit, probably due to the partial loss of solvents from the crystals.

3.2.8 Synthesis of $Co(4)Cl_2{\cdot}C_7H_8$ (10). Ligand **4** (29.1 mg, 0.100 mmol) was dissolved in MeOH/CH_2Cl_2 (8 mL, 1 : 3, v/v) in a 20 mL vial, to which was added a solution of $CoCl_2{\cdot}6H_2O$ (23.8 mg, 0.100 mmol) in MeOH (3 mL). Toluene (1 mL) was then added to the reaction. The mixture was stirred for 5 min at ambient temperature and then allowed to slowly evaporate over one week, after which time X-ray quality crystals were obtained by decanting the solvent. The green block-like crystals were washed with MeOH and then dried in air. Yield: 34.8 mg (68%). UV/Vis λ_{max}/nm (1.00×10^{-5} mol L^{-1}, CH_2Cl_2) 236 ($\varepsilon/10^3$ dm^3 mol^{-1} cm^{-1} 34.2), 287 (24.1), 331 (12.8), 347 (11.7). FT-IR (solid, cm^{-1}): 3443br, 2949m, 1667w, 1614s, 1543w, 1475s, 1452m, 1425s, 1406s, 1289s, 1186s, 1141s, 1038s, 886m, 859s. Anal. calcd for $C_{17}H_{17}Cl_2CoN_8{\cdot}C_7H_8$: C 56.16, H 4.91, N 13.64%. Found C 55.84, H 3.27, N 13.32%.

3.3 General procedure for catalysed alkene hydroboration and hydrosilylation

In a glovebox under a N_2 atmosphere, the metal precatalyst (0.25 μmol, 0.5 mol%) and KO^{t}Bu (1.12 mg, 1 mol%) were suspended in THF (0.5 mL) in a 3.8 mL glass vial equipped with a small stir bar. The mixture was stirred for 1 min. Styrene (1.0 mmol) and pinacolborane or phenylsilane (1.1 mmol) were then added. The reaction mixture was allowed to stir at room temperature for 16 h and then the reaction was quenched by exposing the reaction solution to air and adding CH_2Cl_2 (1 mL) to the solution. The crude reaction mixture was analysed by GC-MS to determine the total yield of the products as well as the ratio of regioisomeric products by comparing the GC traces with those of authentic samples reported previously.[41]

3.4 Cytotoxicity measurement

Three cell lines used for this study, the non-tumorigenic human mammary epithelial cell line (MCF-10A), the breast cancer cell line (MCF-7), and the triple-negative breast cancer cell line (MDA-MB-468), were obtained from ATCC. The cells were maintained in an incubator with 5% CO_2 at 37 °C. The culture media of MCF-10A cells contained Dulbecco's modified Eagle's medium (DMEM) with 5% fetal bovine serum (FBS), 50 μg mL^{-1} gentamicin and a mixture of supplements: 10 μg mL^{-1} human insulin, 20 ng mL^{-1} hEGF, 100 ng mL^{-1} cholera toxin, and 0.5 μg mL^{-1} hydrocortisone. The culture media of MCF-7 contained DMEM with 10% FBS and 50 μg mL^{-1} gentamicin. The culture media of MDA-MB-468 contained DMEM with 10% FBS, 2 mM L-glutamine and 50 μg mL^{-1} gentamicin. The cells were cultured in 96-well plates with a seeding density of 1×10^4 cells per well to ensure that there is about 80% confluence when exposed to chemicals on the day prior to chemical treatment. A 100 mM stock solution for each compound was prepared by using dimethyl sulfoxide (DMSO) as a solvent. Chemical treatment solutions (0 to 100 μM) for each compound were then diluted from the stock solution in the culture media. The highest concentration of DMSO in the solution was 0.1%, which was generally considered non-toxic to cells. The cytotoxicity was determined using a CCK-8 cytotoxicity assay following the manufacturer's protocol (Sigma-Aldrich). The absorbance signals were detected using a BioTek Cytation 7 cell imaging multimode reader at 450 nm. Three separate experiments were conducted for statistical analysis. IC_{50} was calculated using AAT Bioquest analysis (https://www.aatbio.com/tools/ic50-calculator (accessed on October 28, 2025)).

3.5 X-ray crystallography

X-ray diffraction data were collected using a Bruker X8 Kappa Apex II (for **3**, **6**, **7** and **9**), a Bruker D8 Venture (for **4**, **5** and **8**) or a Bruker APEX II CCD (for **10**) diffractometer using Mo Kα radiation. Crystal data, data collection and refinement parameters are summarized in Table S1 (see the SI). The structures were solved by direct methods or using a dual-space method and standard difference map techniques and were refined by full-matrix least-squares procedures on F^2 with SHELXTL.[42,43] All hydrogen atoms bound to carbon were placed in calculated positions and refined with a riding model [U_{iso}(H) = 1.2–1.5U_{eq}(C)], while hydrogen atoms bound to oxygen were located on the difference map and freely refined. SQUEEZE/PLATON was used to treat the disordered solvent as a diffuse contribution to the overall scattering for **9**.[44,45] CCDC 2391278 and 2497364–2497370 contain the supplementary crystallographic data for this paper.

Author contributions

G. Z. and S.-Y. C. conceived the project. H. M., M. C., P. H and A. K. performed experimental studies and analysed the data. M. C. N. conducted the X-ray crystallographic analysis of compounds **3**, **6**, **7** and **9**. G. Z. and S.-Y. C. wrote the manuscript. G. Z., A. K. and M. C. N. revised the manuscript.

Conflicts of interest

There are no conflicts to declare.

Data availability

Data supporting this article have been included as part of the supplementary information (SI). Supplementary information: Table S1 and Fig. S1–S18 for crystallograhic data, UV-Vis, FT-IR, MS and NMR spectra and additional crystal structures. See DOI: https://doi.org/10.1039/d5dt02824h.

CCDC 2391278 and 2497364–2497370 contain the supplementary crystallographic data for this paper.[46a–h]

Acknowledgements

We are grateful for the financial support from the National Science Foundation (CHE-2247728) for this work. We are also thankful for the support from the American Chemical Society Petroleum Research Fund (#66150-UR1). The PRISM program at John Jay College, the City University of New York, is gratefully acknowledged. Dr. James A. Golen (UMass Dartmouth) and Dr. James C. Fettinger (UC Davis) are gratefully acknowledged for X-ray crystallographic analysis of **4**, **5**, **8** and **10**.

References

1 H. A. Favre and W. H. Powell, *Nomenclature of organic chemistry: IUPAC recommendations and preferred names 2013*, Royal Society of Chemistry, Cambridge, UK, 2013, Rule P-16.4.
2 U. S. Schubert, H. Hofmeier and G. R. Newkome, *Modern terpyridine chemistry*, Wiley-VCH Verlag & Co., Weinheim, Germany, 2006.
3 A. M. C. Thompson, The synthesis of 2,2′:6′,2″-terpyridine ligands – versatile building blocks for supramolecular chemistry, *Coord. Chem. Rev.*, 1997, **160**, 1–52.
4 M. Heller and U. S. Schubert, Syntheses of functionalized 2,2′:6′,2″-terpyridines, *Eur. J. Org. Chem.*, 2003, 947–961.
5 E. C. Constable, 2,2′:6′,2″-Terpyridines: from chemical obscurity to common supramolecular motifs, *Chem. Soc. Rev.*, 2007, **36**, 246–253.
6 B. Z. Momeni, N. Davarzani, J. Janczak, N. Ma and A. S. Abd-El-Aziz, Progress in design and applications of supramolecular assembly of 2,2′:6′,2″-terpyridine-based first-row d-block elements, *Coord. Chem. Rev.*, 2024, **506**, 215619.
7 A. Winter, G. R. Newkome and U. S. Schubert, The chemistry of the s- and p-block elements with 2,2′:6′,2″-terpyridine ligands, *Inorg. Chem. Front.*, 2024, **11**, 342–399.
8 R. R. Panicker and A. Sivaramakrishna, Remarkably flexible 2,2′:6′,2″-terpyridines and their group 8–10 transition-metal complexes – chemistry and applications, *Coord. Chem. Rev.*, 2022, **459**, 214426.
9 S. M. Elahi, M. Raizada, P. K. Sahu and S. Konar, Terpyridine-based 3D metal–organic frameworks: a structure–property correlation, *Chem. – Eur. J.*, 2021, **27**, 5858–5870.
10 A. Winter and U. S. Schubert, Metal–terpyridine complexes in catalytic application – a spotlight on the last decade, *ChemCatChem*, 2020, **12**, 2890–2941.
11 D. Rocco, C. E. Housecroft and E. C. Constable, Synthesis of terpyridines: simple reactions – what could possibly go wrong?, *Molecules*, 2019, **24**, 1799.
12 C. E. Housecroft and E. C. Constable, Isomers of terpyridine as ligands in coordination polymers and networks containing zinc(II) and cadmium(II), *Molecules*, 2021, **26**, 3110.
13 T. N. Francisco, H. M. Albuquerque and A. M. Silva, An in-depth exploration of six decades of the Kröhnke pyridine synthesis, *Chem. – Eur. J.*, 2024, **30**, e202401672.
14 D. J. Bray, J. K. Clegg, K. A. Jolliffe, L. F. Lindoy and G. Wei, Synthesis and co-crystallisation behaviour of copper(II) complexes of two isomeric p-tolyl-terpyridines, *J. Coord. Chem.*, 2008, **61**, 3–13.
15 J.-P. Collin, S. Guillerez, J.-P. Sauvage, F. Barigelletti, L. De Cola, L. Flamigni and V. Balzani, Photoinduced processes in dyads and triads containing a ruthenium(II)-bis(terpyridine) photosensitizer covalently linked to electron donor and acceptor groups, *Inorg. Chem.*, 1991, **30**, 4230–4238.
16 M. L. Turonek, P. Moore and W. Errington, Synthesis of the terpyridyl pendant-arm azamacrocycle 4′-(p-1,4,7-triazacyclonon-1-ylmethylphenyl)-2,2′:6′,2″-terpyridine (L) and complexes of L with copper(II) and nickel(II): crystal structure of $[Cu(HL)(H_2O)_2][PF_6]_3$, *J. Chem. Soc., Dalton Trans.*, 2000, 441–444.
17 E. Rajalakshmanan and V. Alexander, Synthesis, luminescence, and electrochemical studies of tris(homoleptic) ruthenium(II) and osmium(II) complexes of 6′-tolyl-2,2′:4′,2″-terpyridine, *Inorg. Chem.*, 2007, **46**, 6252–6260.
18 D.-Y. Zhang, Y. Nie, H. Sang, J.-J. Suo, Z.-J. Li, W. Gu, J.-L. Tian, X. Liu and S.-P. Yan, Three structurally related copper complexes with two isomers: DNA/BSA binding ability, DNA cleavage activity and excellent cytotoxicity, *Inorg. Chim. Acta*, 2017, **457**, 7–18.
19 H. L. Anderson, S. Anderson and J. K. M. Sanders, Ligand binding by butadiyne-linked porphyrin dimers, trimers and tetramers, *J. Chem. Soc., Perkin Trans. 1*, 1995, 2231–2245.
20 Z. Yin, G. Zhang, T. Phoenix, S. Zheng and J. C. Fettinger, Assembling mono-, di- and trinuclear coordination complexes with a ditopic analogue of 2,2′:6′,2″-terpyridine: syntheses, structures and catalytic studies, *RSC Adv.*, 2015, **5**, 36156–36166.
21 R. Liegghio, P. G. Potvin and A. B. P. Lever, 2,6-Dipyrazinylpyridines and their ruthenium(II) complexes: a new polynucleating ligand family, *Inorg. Chem.*, 2001, **40**, 5485–5486.
22 R. G. Miller, M. R. Warren, D. R. Allan and S. Brooker, Direct crystallographic observation of CO_2 captured in zig-zag channels of a copper(I) metal–organic framework, *Inorg. Chem.*, 2020, **59**, 6376–6381.
23 J. D. Holbrey, G. J. T. Tiddy and D. W. Bruce, Amphiphilic terpyridine complexes of ruthenium and rhodium display-

ing lyotropic mesomorphism, *J. Chem. Soc., Dalton Trans.*, 1995, 1769–1774.
24 M. Maskus and H. D. Abruña, Synthesis and characterization of redox-active metal complexes sequentially self-assembled onto gold electrodes via a new thiol–terpyridine ligand, *Langmuir*, 1996, **12**, 4455–4462.
25 J. Lee, H. Chang, S. Kim, G. S. Bang and H. Lee, Molecular monolayer nonvolatile memory with tunable molecules, *Angew. Chem., Int. Ed.*, 2009, **48**, 8501–8504.
26 B. Cuenoud and A. Schepartz, A general scheme for incorporating nonnatural functionality into peptides, *Tetrahedron Lett.*, 1991, **32**, 3325–3328.
27 E. C. Constable, N. Hostettler, C. E. Housecroft, P. Kopecky, M. Neuburger and J. A. Zampese, 2,2′:6′,2″-Terpyridine substituted in the 4′-position by the solubilizing and sterically demanding tert-butyl group: a surprisingly new ligand, *Dalton Trans.*, 2012, **41**, 2890–2897.
28 E. C. Constable, C. E. Housecroft, P. Kopecky, M. Neuburger, J. A. Zampese and G. Zhang, Coordination polymers with divergent 4′-tert-butyl-4,2′:6′,4″-terpyridine linkers: from aryl–aryl to ball-and-socket packing, *CrystEngComm*, 2012, **14**, 446–452.
29 G. Zhang, H. Zeng, J. Wu, Z. Yin, S. Zheng and J. C. Fettinger, Highly Selective Hydroboration of Alkenes, Ketones and Aldehydes Catalyzed by a Well-Defined Manganese Complex, *Angew. Chem., Int. Ed.*, 2016, **55**, 14369–14372.
30 G. Zhang, J. Wu, S. Li, S. Cass and S. Zheng, Markovnikov-Selective Hydroboration of Vinylarenes Catalyzed by a Cobalt (II) Coordination Polymer, *Org. Lett.*, 2018, **20**, 7893–7897.
31 J. Wu, H. S. Zeng, J. Cheng, S. P. Zheng, J. A. Golen, D. R. Manke and G. Zhang, Cobalt(II) Coordination Polymer as a Precatalyst for Selective Hydroboration of Aldehydes, Ketones, and Imines, *J. Org. Chem.*, 2018, **83**, 9442–9448.
32 G. Zhang, J. Wu, S. Zheng, M. C. Neary, J. Mao, M. Flores, R. J. Trovitch and P. A. Dub, Redox-Noninnocent Ligand-Supported Vanadium Catalysts for the Chemoselective Reduction of C=X (X = O, N) Functionalities, *J. Am. Chem. Soc.*, 2019, **141**, 15230–15239.
33 G. Zhang, S. Zheng and M. C. Neary, An ionic Fe-based metal–organic-framework with 4′-pyridyl-2,2′:6′,2″-terpyridine for catalytic hydroboration of alkynes, *RSC Adv.*, 2023, **13**, 2225–2232.
34 G. Zhang, H. Zeng, N. Zadori, C. Marino, S. Zheng and M. C. Neary, Homoleptic octahedral CoII complexes as pre-catalysts for regioselective hydroboration of alkenes with high turnover frequencies, *RSC Adv.*, 2023, **13**, 28089–28096.
35 G. Zhang, J. Tan, Y. Z. Zhang, C. Ta, S. Sanchez, S. Y. Cheng, J. A. Golen and A. L. Rheingold, Syntheses, structures and cytotoxicity of cobalt(II) complexes with 4′-chloro-2,2′:6′,2″-terpyridine, *Inorg. Chim. Acta*, 2015, **435**, 147–152.
36 X. Chen, Q. Zhang, A. Kaswer, H. Kim, M. Ahmed, M. C. Neary, S. Y. Cheng, G. Zhang and J. M. Rauceo, Indium(III)–terpyridine, complexes: synthesis, structures and remarkable antifungal and anticancer activities, *Dalton Trans.*, 2025, **54**, 4656–4663.
37 E. Rajalakshmanan and V. Alexander, Synthesis, luminescence, and electrochemical studies of tris(homoleptic) ruthenium(II) and osmium(II) complexes of 6′-tolyl-2,2′:4′,2″-terpyridine, *Inorg. Chem.*, 2007, **46**, 6252–6260.
38 C. E. Housecroft and E. C. Constable, Does the central nitrogen atom make a difference? A comparison of non-coordinating pyridine and benzene spacers in multitopic ligands, *Helv. Chim. Acta*, 2024, **107**, e202400023.
39 R. Musiol, P. Malecki, M. Pacholczyk and J. Mularski, Terpyridines as promising antitumor agents: an overview of their discovery and development, *Expert Opin. Drug Discovery*, 2022, **17**, 259–271.
40 R. Abhijnakrishna, K. Magesh, A. Ayushi and S. Velmathi, Advances in the biological studies of metal-terpyridine complexes: an overview from 2012 to 2022, *Coord. Chem. Rev.*, 2023, **496**, 215380.
41 G. Zhang, H. Zeng, S. Li, J. Johnson, Z. Mo, M. C. Neary and S. Zheng, 1-D manganese(II)-terpyridine coordination polymers as precatalysts for hydrofunctionalisation of carbonyl compounds, *Dalton Trans.*, 2020, **49**, 2610–2615.
42 G. M. Sheldrick, *SHELXTL, An Integrated System for Solving, Refining, and Displaying Crystal Structures from Diffraction Data*, University of Göttingen, Göttingen, Federal Republic of Germany, 1981.
43 G. M. Sheldrick, SHELXT-Integrated Space-Group and Crystal-Structure Determination, *Acta Crystallogr., Sect. A: Found. Adv.*, 2015, **71**, 3–8.
44 A. L. Spek, *PLATON, A Multipurpose Crystallographic Tool*, 2005, Utrecht University, Utrecht, The Netherlands.
45 A. L. Spek, Single-crystal structure validation with the program PLATON, *J. Appl. Crystallogr.*, 2003, **36**, 7–13.
46 (*a*) CCDC 2391278: Experimental Crystal Structure Determination, 2026, DOI: 10.5517/ccdc.csd.cc2l8b07; (*b*) CCDC 2497364: Experimental Crystal Structure Determination, 2026, DOI: 10.5517/ccdc.csd.cc2ptq4d; (*c*) CCDC 2497365: Experimental Crystal Structure Determination, 2026, DOI: 10.5517/ccdc.csd.cc2ptq5f; (*d*) CCDC 2497366: Experimental Crystal Structure Determination, 2026, DOI: 10.5517/ccdc.csd.cc2ptq6g; (*e*) CCDC 2497367: Experimental Crystal Structure Determination, 2026, DOI: 10.5517/ccdc.csd.cc2ptq7h; (*f*) CCDC 2497368: Experimental Crystal Structure Determination, 2026, DOI: 10.5517/ccdc.csd.cc2ptq8j; (*g*) CCDC 2497369: Experimental Crystal Structure Determination, 2026, DOI: 10.5517/ccdc.csd.cc2ptq9k; (*h*) CCDC 2497370: Experimental Crystal Structure Determination, 2026, DOI: 10.5517/ccdc.csd.cc2ptqbl.